Available online at www.sciencedirect.com
SCIENCE DIRECT
Electrochimica Acta 51 (2006) 3736–3742
ELECTROCHIMICA Acta
www.elsevier.com/locate/electacta

# Brass dezincification in a tap water bacterial suspension

M.B. Valcarce, S.R. de Sánchez, M. Vázquez *,[1]

*División Corrosión, INTEMA, Facultad de Ingeniería, UNMdP, Juan B. Justo 4302, B7608FDQ Mar del Plata, Argentina*

Received 19 August 2005; received in revised form 19 October 2005; accepted 19 October 2005
Available online 7 December 2005

**Abstract**

The dezincification of Al–brass under the influence of *Pseudomona fluorescens* in potable water is investigated.

The experiments were carried out using artificial tap water, pH 7.6. For comparison, a bacterial suspension, was also used. Potentiodynamic reduction curves, polarization curves, polarization resistance and impedance spectroscopy as well as reflectance spectroscopy were used to characterise the surface films grown at open circuit potential.

The dezincification associated to the presence of bacteria was revealed by changes in the reduction curves, and also by changes in the reflectance spectra. No significant differences were observed between the fitting parameters of the impedance spectra.

The Tafel slopes were found to increase in the bacterial suspension. The corrosion currents are higher than in the inoculated electrolyte, particularly in the case of brass. This increment is attributed to the higher Tafel slope and is taken as an indication of the dezincification phenomenon.


*Keywords:* Copper alloy; Corrosion; Optical reflectivity; Electrochemistry; Dealloying

## 1. Introduction

Microbiologically influenced corrosion is a common problem associated to tap water distribution systems, particularly when copper and copper alloys are the construction materials [1–3].

When a biofilm develops on copper alloys, the passive state is compromised and the oxygen reduction rate has been found to increase [4]. The increment can lead to the ennoblement of the corrosion potential [5,6], contributing to the onset of localized corrosion.

In the case of copper, bacterial growth can trigger the development of localized corrosion, such as pitting [2,3,7]. Yet, the dezincification of the surface is another characteristic type of localized attack that is observed on zinc-rich copper alloys, which can be associated to the presence of microorganisms [7–10]. The dezincification process involves the dissolution of the most active component, in this case the zinc, leaving on the surface of the alloy a fragile layer rich in copper, which is the noblest component.

Pseudomonas are commonly isolated from biofilms that develop on copper in drinkable water conduction systems [11–13]. These bacteria have been broadly associated to microbiological corrosion problems [4–7,14–17]. They present a high resistance to the toxic effect of the cupric ions ($Cu^{2+}$) dissolved into the solution as a result of the corrosive process. In this context, and complementing the results from a previous publication where the stress was on pitting, the present paper deals with the dezincification of Al–brass under the influence of *Pseudomona fluorescens* in drinkable water.

## 2. Materials and methods

The experimental set-up used to carry out this investigation is described in detail elsewhere [7]. A brief description of the most relevant facts is presented below.

### 2.1. Electrolyte composition

All the experiments were carried out using artificial tap water (ATW). The pH was adjusted to 7.6 with HCl solution 1 mol $l^{-1}$.

To evaluate the effect of the presence of bacteria, pure cultures of *P. fluorescens* (ATCC 17552) were grown at 32 °C. Cells were harvested from cultures at the mid-exponential phase of growth,

* Corresponding author. Tel.: +54 223 481 6600; fax: +54 223 481 0046.
*E-mail address:* mvazquez@fi.mdp.edu.ar (M. Vázquez).
[1] ISE active member.

0013-4686/$ – see front matter © 2005 Elsevier Ltd. All rights reserved.
doi:10.1016/j.electacta.2005.10.034

washed and suspended in ATW after centrifuging again. This bacterial suspension was labelled as "BATW".

All the experiments were carried out at room temperature ($20 \pm 2\,^{\circ}C$).

### 2.2. Electrodes preparation

The specimens for electrochemical evaluation consisted of disc samples of aluminium brass (Al–brass, UNS 68700) and copper, included in fast curing acrylic resin on appropriated PVC holders. Samples were abraded to grade 600 with emery paper, and mirror polished with 0.05 μm alumina powder (Type B-Buehler, Lake Bluff, USA). The geometrical area exposed was 0.312 $cm^2$ in the case of copper and 0.554 $cm^2$ for brass.

For all the electrochemical tests in ATW or BATW, the electrodes were prereduced in the electrolyte at −1.1 V for 15 min to obtain a reproducible, clean surface. After that, the passive film was grown on the metallic surfaces at the open circuit potential for 2 h. These samples will be referred to as "aged" samples.

### 2.3. Electrochemical techniques

A Voltalab™ PGZ 100 potentiostat and a Solartron™ SI 1280B unit were used to perform the electrochemical experiments.

A three-electrode electrochemical cell was used. A saturated calomel electrode (SCE, $E = 0.24$ V versus NHE) was used as reference and a platinum wire of large area as counter electrode.

Anodic and cathodic potentiodynamic curves carried out in deareated ATW applying a potentiodynamic scan at a rate of 0.1 or 10 mV $s^{-1}$. The starting point was the potential where the oxide had been grown. The corrosion current density was also evaluated from the intersection of the polarization curves recorded in independent experiments using two different electrodes.

Polarization resistance ($R_{p\,sweep}$) was evaluated as $\Delta V/\Delta i$, from potential sweeps up to ±0.01 V from $E_{corr}$ at a scan rate of $10^{-4}$ V $s^{-1}$. The corrosion rate was evaluated from the polarization resistance data according to the Stern–Geary relationship [18] as:

$$i_{corr} = \frac{\beta_a \beta_c}{2.303(\beta_a + \beta_c)} \frac{1}{R_p} = \frac{B}{R_p} \quad (1)$$

where $\beta_a$ and $\beta_c$ are the anodic and cathodic Tafel slopes, respectively, which are kinetic parameters characteristic of each metal-solution system.

Electrochemical impedance spectra were performed at open circuit potential (OCP). Recording each spectrum took between 90 and 160 min. The ac voltage signal amplitude was ±0.01 V and the frequency varied between 20 kHz and 1 mHz. The solution was used without stirring or deareation. The results were analyzed using the equivalent circuit presented in Fig. 1. $R_s$ represents the solution resistance, $Z_{CPE0}$ the constant phase element of the surface oxide, $R_0$ the resistance to current flow through defects in the surface oxide, $Z_{CPEdl}$ the constant phase element of the double layer and $R_{dl}$ is the polarization resistance. This circuit is typical of oxide-coated metals and has been used

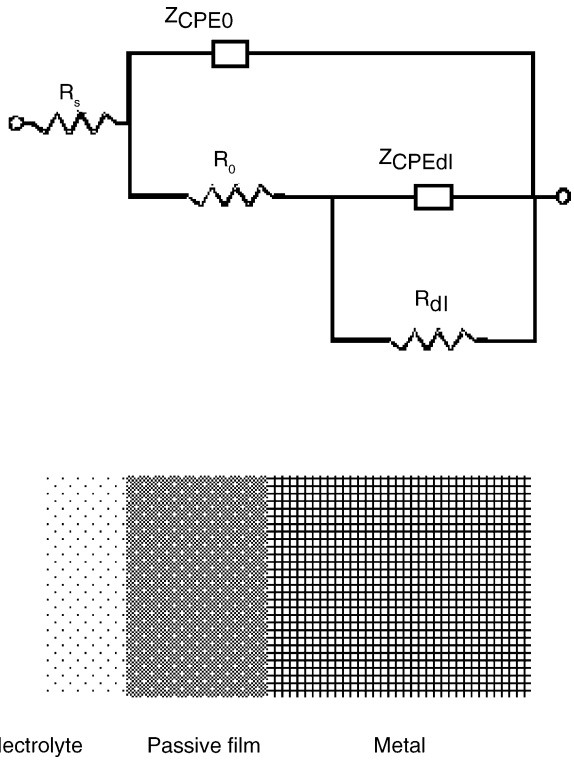


Fig. 1. Equivalent circuit proposed for interpreting the EIS response.

before by other authors in relation to copper corrosion in potable water [19,20]. Corroding electrodes can show various types of inhomogeneities, which can be better represented by the inclusion of constant phase elements (CPE) instead of capacitors in the equivalent circuit. Surface roughness, insufficient polishing, grain boundaries and surface impurities had been mentioned before among the main reasons that justify the use of CPEs in equivalent circuits of corroding electrodes [21]. The impedance of this element is frequency-dependent, and can be mathematically expressed using two parameters, $Q$ and $n$ as:

$$Z_{CPE} = [Q(j\omega)^n]^{-1} \quad (2)$$

where $Q$ is the frequency-independent real constant or pseudo-capacitance and $n$ is a constant power, with $-1 < n < 1$. A rough or porous surface can cause a double layer capacitance to appear as a constant phase element with $n$ between 0.5 and 1.

### 2.4. Spectroscopic techniques

UV–visible reflectance spectroscopy was carried out using a commercial double-beam spectrophotometer (Shimadzu UV 160A) conveniently modified as described elsewhere [22,23]. The absorption spectra were then recorded in situ. Baseline corrections were carried out by polarising two identical polished surfaces at −1.1 V to prevent oxide growth. This baseline ($R_0$) was subtracted from each of the following spectra so as to show changes in reflectance, as a function of wavelength. To evaluate the effect of the presence of bacteria on the surface films, the electrolyte was replaced by BATW after recording the base-

line. The electrodes where then aged at open circuit potential for 2 h. To avoid interferences in the absorption signal, the solution was replaced again with ATW prior to recording the reflectance spectra.

## 3. Results

### *3.1. Surface films characterization by potentiodynamic reduction curves*

Both copper and brass reach the steady-state open circuit potential (OCP) after 2 h of immersion in ATW or BATW. In the case of brass, the OCP stabilizes at around −0.011 V in ATW and −0.021 V in BATW; while in the case of copper the OCP is around −0.039 V in ATW and −0.010 V in BATW.

The effect of the presence of bacteria in the electrolyte on the composition of the surface films formed at open circuit potentials was investigated. Potentiodynamic reduction curves of brass electrodes aged, with and without bacteria, are compared in Fig. 2. The curve obtained in ATW shows characteristic features typical of those described before for films grown at various anodic potentials [7]. The two cathodic peaks at −0.67 and −0.88 V can be attributed to the reduction of cuprous compounds and the reduction of Zn(II) species, respectively. In the presence of bacteria, the peak assigned to Cu(I) species shifts in the positive direction, while the peak ascribed to Zn(II) species is no longer evident. This result suggests that the passive layer looses Zn(II) when it is formed in the presence of bacteria in the electrolyte.

When the film grown on copper is potentiodynamically reduced in ATW, a single cathodic peak appears at −0.66 V, which can be assigned to the reduction of Cu(I) species. The presence of bacteria while the surface layer is growing seems to have no effect on the potentiodynamic reduction curves, other a small shift in the potential of the current peak (30 mV in the positive direction).

In an independent experiment, air was bubbled during the ageing process in the presence of bacteria in order to compensate for the oxygen consumption in the solution resulting from

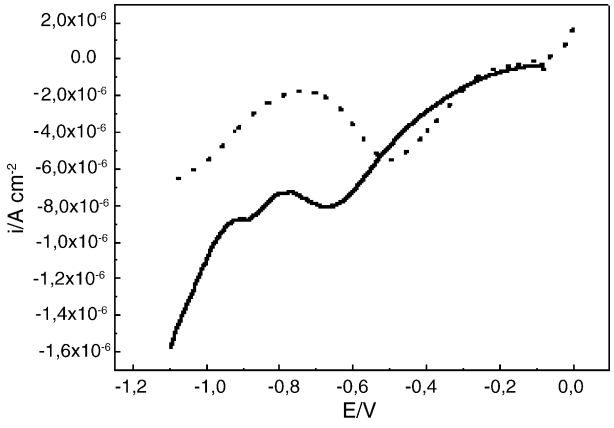


Fig. 2. Potentiodynamic reduction of the surface film grown on brass aged for 2 h at open circuit potential (OCP) in ATW (—) and BATW (- - -). Scan rate: 10 mV $s^{-1}$.

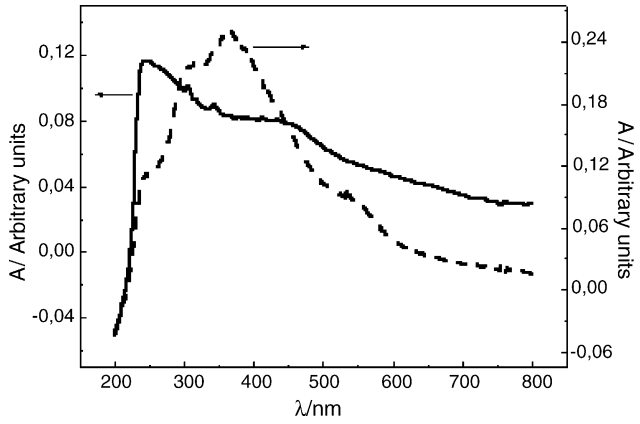


Fig. 3. Reflectance spectra of brass (—) and copper (- - -) held at open circuit potential for 2 h in ATW.

cell respiration. No differences were observed in the potentiodynamic reduction curves in any of both materials.

### *3.2. Surface films characterization by reflectance spectroscopy*

Fig. 3 presents the comparison between the spectra of Cu and brass aged in ATW. For brass, a broad peak at 462 nm, a lower one at 360–380 nm and a shoulder at 237 nm suggest the presence of $Cu_2O$ [17,22,23]. There is also a peak at 260 nm, corresponding to the main absorption feature of the zinc oxohydroxides [17,24]. In the case of copper, typical absorbance peaks that can be seen at 237, 314 and 380 nm together with shoulders at 462 and 550 nm [22,23].

Fig. 4 compares the spectra of Cu and brass aged in BATW and confirm dezincification. The spectrum of Cu remains practically the same as that in Fig. 3. For brass, however, a broad peak appears between 330 and 480 nm. This has been attributed before to a surface layer enriched in copper [25]. Also, the relative intensity of the Zn(II) peak at 260 nm decreases, in agreement with the selective dissolution of Zn from the passive layer, proposed above. The relative intensities of the peaks should be considered within each particular spectrum because the absorption scale has

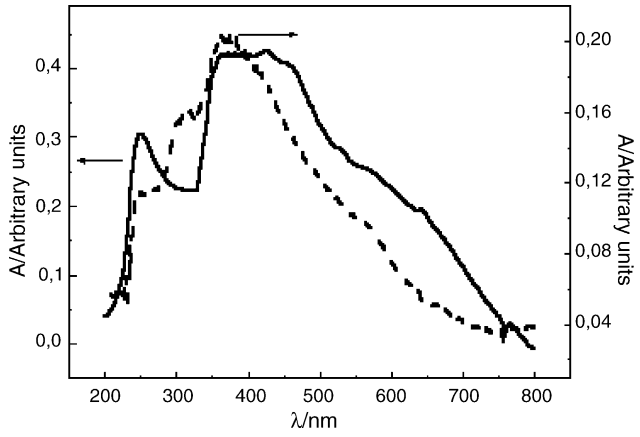


Fig. 4. Reflectance spectra of brass (—) and copper (- - -) held at open circuit potential for 2 h in BATW.

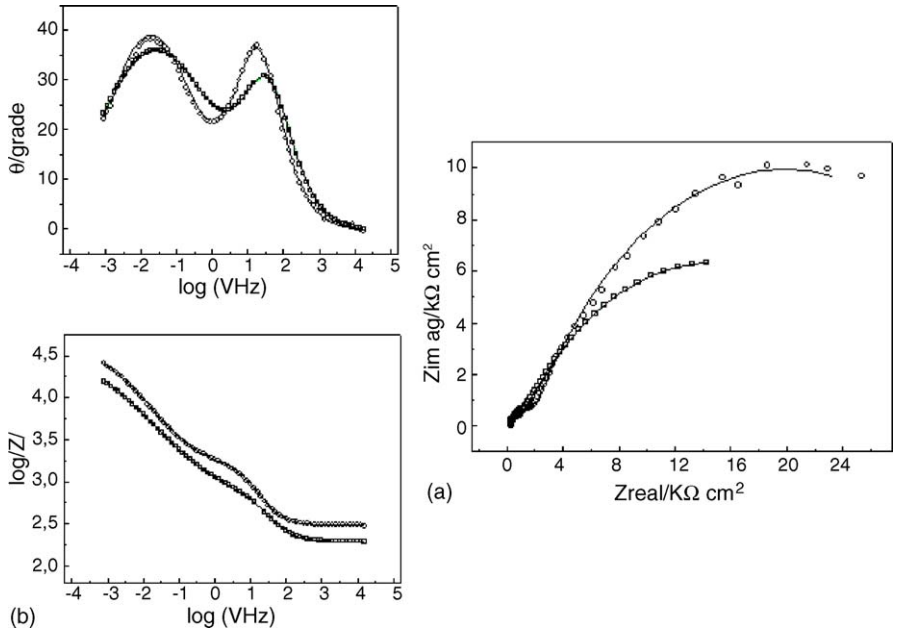


Fig. 5. Impedance spectra recorded on brass electrodes held for 2 h at OCP in ATW (□) and BATW (◯). The symbols represent the data and the lines the fitting results (see Fig. 1 for the equivalent circuit). (a) Nyquist representation and (b) Bode representation.

arbitrary units, as it depends on the light path and thus on the position of the sample in the cell.

### 3.3. Characterization of the surface films by electrochemical impedance spectroscopy

The results of the impedance spectra recorded on brass and copper, are shown in Figs. 5 and 6, respectively. The comparison between electrodes aged in ATW or BATW is presented. The impedance spectra present two time constants. An schematic representation of the structure of the surface film present after ageing in ATW and the corresponding equivalent circuit were presented in Fig. 1.

EIS data fit results are also shown in Figs. 5 and 6. The experimental data were found to be sufficiently well fitted by the proposed circuit. Table 1 presents the optimised values for the various parameters involved.

From the $R_p$ values (Table 2), the corrosion current density was calculated using Eq. (1). The results are shown in Table 3.

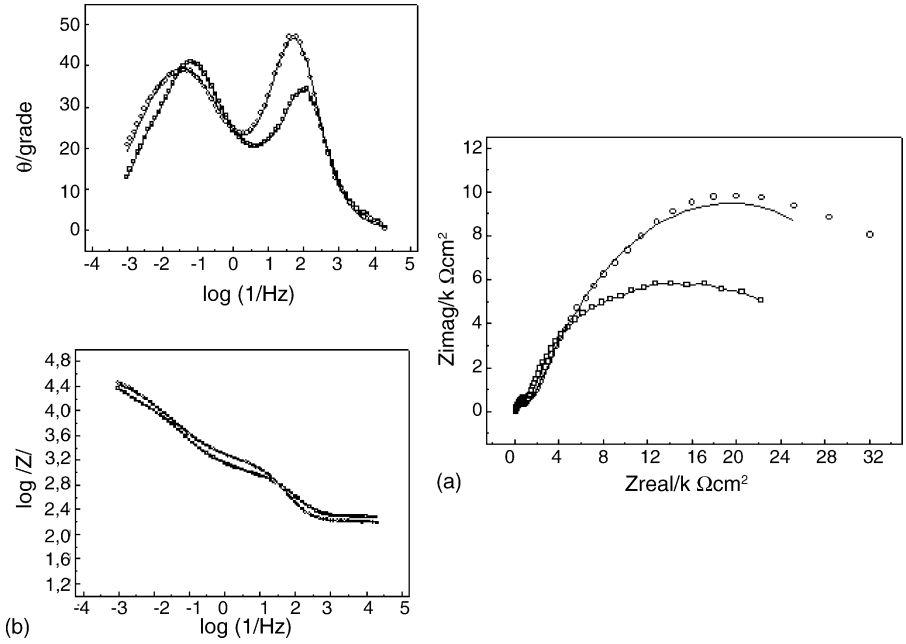


Fig. 6. Impedance spectra recorded on copper electrodes held for 2 h at OCP in ATW (□) and BATW (◯). The symbols represent the data and the lines the fitting results (see Fig. 1 for the equivalent circuit). (a) Nyquist representation; (b) Bode representation.

Table 1
Optimised parameters to fit the data in Figs. 5 and 6 with the equivalent circuit in Fig. 1

| Element | Brass ATW | Copper ATW | Brass BATW | Copper BATW |
|---|---|---|---|---|
| $R_s$ ($\Omega\,cm^2$) | 208 | 192 | 281 | 161 |
| $Q_0$ ($\Omega^{-1}\,cm^{-2}\,s^N$) | $3.1 \times 10^{-5}$ | $1.2 \times 10^{-5}$ | $2.9 \times 10^{-5}$ | $1.2 \times 10^{-5}$ |
| $n_0$ | 0.81 | 0.85 | 0.85 | 0.89 |
| $R_0$ ($\Omega\,cm^2$) | 767 | 809 | 1203 | 1255 |
| $Q_{dl}$ ($\Omega^{-1}\,cm^{-2}\,s^N$) | $3.3 \times 10^{-4}$ | $5.6 \times 10^{-4}$ | $5.9 \times 10^{-4}$ | $4.6 \times 10^{-4}$ |
| $n_{dl}$ | 0.57 | 0.66 | 0.62 | 0.58 |
| $R_{dl}$ ($\Omega\,cm^2$) | 29891 | 24739 | 30374 | 33701 |

Table 2
Polarization resistance values for copper and brass aged at OCP, averaged from at least three experiments

| | $R_{p\,EIS}$ ($\Omega\,cm^{-2}$) | $R_{p\,sweep}$ ($\Omega\,cm^{-2}$) |
|---|---|---|
| Brass | | |
| ATW | 29890 | 24470 |
| BATW | 30370 | 30500 |
| Copper | | |
| ATW | 24740 | 23110 |
| BATW | 33700 | 20390 |

### 3.4. Characterization of the surface films in terms of corrosion resistance

Anodic and cathodic polarization curves for brass and copper are presented in Figs. 7 and 8, respectively. The results recorded for electrodes aged in ATW and BATW are shown superimposed. The corrosion current, determined from their intercepts, is presented in Table 3. The current increment in the positive end of the anodic polarization curves is related to the appearance of pitting and it has been discussed in more detail elsewhere [7].

Also, Tafel slopes can be evaluated as the slope of the linear portion of $E$ versus log ($i$) curves. Calculated Tafel slopes values, together with the resulting value for the coefficient $B$ in Eq. (1) are summarized in Table 4. Badawy et al. [26] assumed Tafel slopes of 0.12 V and $B = 0.026$ V for a lead–brass alloy in neutral solutions.

Table 3
Corrosion current density values for copper and brass aged at OCP

| | $i_{corr\,EIS}$ ($A\,cm^{-2}$) | $i_{corr\,pol}$ ($A\,cm^{-2}$) | $i_{corr\,R_p}$ ($A\,cm^{-2}$) |
|---|---|---|---|
| Brass | | | |
| ATW | $3.7 \times 10^{-7}$ | $2 \times 10^{-7}$ | $4.5 \times 10^{-7}$ |
| BATW | $7.6 \times 10^{-7}$ | $4 \times 10^{-7}$ | $7.5 \times 10^{-7}$ |
| Copper | | | |
| ATW | $8.1 \times 10^{-7}$ | $3.5 \times 10^{-7}$ | $8.6 \times 10^{-7}$ |
| BATW | $7.4 \times 10^{-7}$ | $5.4 \times 10^{-7}$ | $1.2 \times 10^{-6}$ |

$i_{corr\,EIS}$ is calculated after fitting EIS results with the equivalent circuit in Fig. 1. $i_{corr\,pol}$ is calculated from the interception of the polarization curves in Figs. 7 and 8. $i_{corr\,R_p}$ is calculated from the polarization resistance measurements.

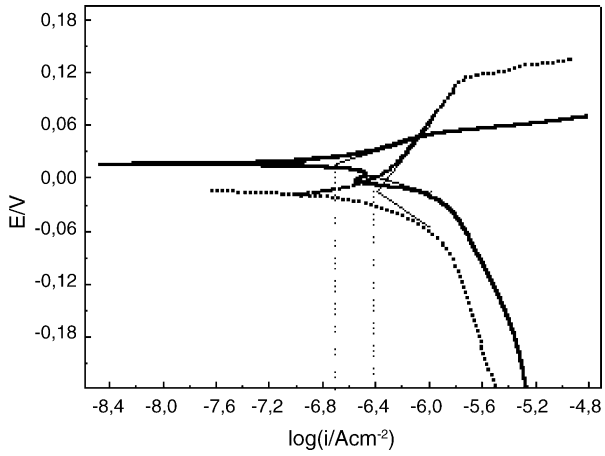


Fig. 7. Anodic and cathodic polarization curves for brass. The curves were recorded after holding the electrodes 2 h at OCP in ATW (—) and BATW (- - -). Each curved started at OCP. Scan rate: 0.1 mV $s^{-1}$.

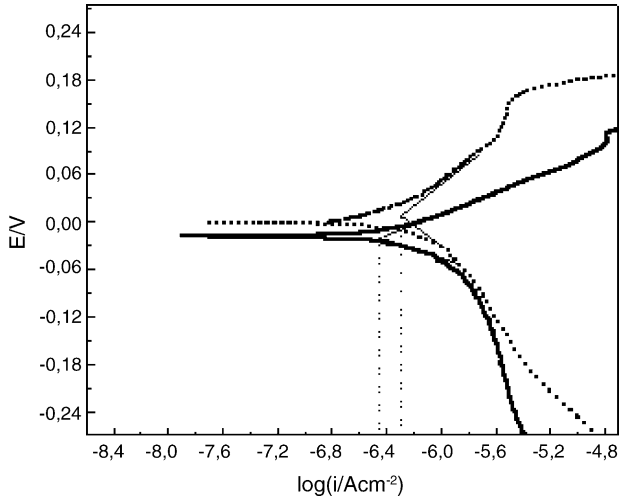


Fig. 8. Anodic and cathodic polarization curves for copper. The curves were recorded after holding the electrodes 2 h at OCP in ATW (—) and BATW (- - -). Each curved started at OCP. Scan rate: 0.1 mV $s^{-1}$.

The polarization resistance can also be calculated from potential sweeps in the vicinity of the OCP (see Table 2). From these, the corrosion current is calculated as described in Section 2.3. In Table 3, they are compared with corrosion current density values that had been calculated from EIS.

Table 4
Tafel slopes evaluated from of the linear portion of the polarization curves (Figs. 7 and 8)

| | $\beta_c$ (V) | $\beta_a$ (V) | $B$ (V) |
|---|---|---|---|
| Brass | | | |
| ATW | 0.054 | 0.045 | 0.011 |
| BATW | 0.072 | 0.211 | 0.023 |
| Copper | | | |
| ATW | 0.104 | 0.079 | 0.020 |
| BATW | 0.123 | 0.111 | 0.025 |

$B = \frac{\beta_a \beta_c}{2.303(\beta_a + \beta_c)}$.

## 4. Discussion

On Al–brass, the dezincification associated to the presence of bacteria was revealed by the disappearance of the peak attributed to Zn(II) reduction in the potentiodynamically reduction curves (Fig. 2), as well as by changes in the absorption of light (Fig. 4). On copper, on the other hand, the film does not show differences neither in the composition nor in the thickness, resulting from the presence or not of bacteria in the electrolyte. Differential reflectance spectroscopy combines optics and electrochemistry, which can be used to identify in situ the composition of thin corrosion films. The light beam penetrates between 50 and 100 atomic layers in a semi-transparent solid. So, this technique is useful to identify changes in the superficial film that may not be detected by other surface techniques.

The dezincification observed on aluminium brass does not seem to be an effect associated to the inhibition of the oxide growth caused by a decrease of the oxygen content due to bacterial respiration.

The impedance spectra were interpreted using an equivalent circuit that represents the electrode/electrolyte interface. By comparing different sets of fitting parameters (like those in Table 1 for a single experiment), no significant differences could be observed comparing brass and copper in either ATW or BATW.

The $R_p$ values obtained by potential sweeps and by EIS were in good agreement. No significant differences were observed between the $R_p$ values with and without bacteria for both materials (Table 2). Other authors reported a decrease in $R_p$ values coinciding with the initiation of the dezincification process [10], but this investigation was carried out using admiralty brass and prolonged immersion periods (over 500 days).

The Tafel slopes, together with the values of the coefficient $B$ are presented in the Table 4. The anodic slope obtained for copper in ATW is in excellent agreement with that measured by Feng et al. in drinkable water [27]. Due to the low Cu(I) solubility in ATW, the oxidation process for copper can be represented as:

$$Cu + OH^- \rightarrow Cu(OH)_{ads} + e^- \quad (3)$$

As one electron is exchanged in the process, the theoretical Tafel slope would be 60 mV [4]. Deviations from this value can be attributed to imperfections in the film structure, such as porosity.

In the case of copper, there is no big difference between the slope values measured in ATW or in BATW. However, in the case of brass a remarkable increment can be appreciated in the anodic Tafel slopes when BATW is compared to ATW ($\beta_a = 0.045$ V in ATW and 0.211 V in BATW). The corrosion process of the alloy is definitively more complex. Furthermore, the polarization curves on brass in BATW were recorded on aged electrodes, i.e. on a surface that was already enriched in copper (dealloyed). In this case, some authors suggest that the anodic processes can involve diffusion of zinc from underlying layers through a porous copper-rich layer [28–30]. Other authors suggest the occurrence of surface diffusion of copper atoms on the alloy surface, so as to fill vacancies and minimize the surface energy [31,32]. In any case, diffusion processes in the surface film could account for the increment in the Tafel slopes when brass has been aged in BATW. Yet, it has to be taken into account that most of the research dealing with Zn selective dissolution on brass has been carried out in electrolytes which are highly acidic or with high levels of chloride ions concentration. Also, it is important to bare in mind the distinction between spontaneous and anodic dissolution of brass proposed by Burzynska [33]. The type of dealloying that corresponds to the system here investigated should be classified as spontaneous (induced by the microorganisms at rest potential). In contrast most of the literature deals with anodic dissolution, where complexing agents play a key role.

The corrosion current density for both materials was calculated from the interception of the polarization curves as well as by means of polarization resistance using Eq. (1). The results are compared in Table 3. The values calculated form the different techniques are in reasonable agreement. The corrosion currents in BATW are higher than those in ATW, particularly for brass. This increment could be attributed to the higher values of the Tafel slope in the presence of bacteria. Within the present experimental conditions, this increment in the corrosion rate resulting from a 2 h contact with a bacterial suspension can be taken as indicative of the initiation of the dezincification phenomenon. This is particularly interesting, given the short time of exposure to the bacterial suspension.

## 5. Conclusions

When brass is aged for 2 h at open circuit potential in contact with a suspension of *Pseudomonas*, reflectance spectroscopy and potentiodynamic reduction curves show evidences of zinc selective dissolution.

In the presence of bacteria the corrosion rates were found to be, in general, higher than in the unpolluted electrolyte. The current increment is more important for brass. This is attributed to the marked increment in the anodic Tafel slope in the presence of bacteria. This increment in the corrosion rate can be taken as indicative for the initiation of the dezincification process.

## Acknowledgements

This work has been supported by the National Research Council of Argentina (CONICET) (PIP2570) and by the Universidad Nacional de Mar del Plata (Grant 15/G115).

## References

[1] B.J. Webster, S.E. Werner, D.B. Weels, P.J. Bremer, Corrosion 56 (9) (2000) 942–950.
[2] P. Bremer, G. Geesey, Appl. Environ. Microbiol. 57 (7) (1991) 1956–1962.
[3] D. Wagner, A.H.L. Chamberlain, Biodegradation 8 (1997) 177–187.
[4] D.J. Schiffrin, S.R. Sánchez, Corrosion 41 (1) (1985) 31–38.
[5] J.P. Busalmen, M.A. Frontini, S.R. Sánchez, Microbial corrosion of microbial catalasa, in: Developments in Marine Corrosion, Campbell and Walsh, Portsmouth, 1995.

[6] J.P. Busalmen, M. Vázquez, S.R. Sánchez, Electrochim. Acta 47 (2002) 1857–1865.
[7] M.B. Valcarce, S.R.d. Sánchez, M. Vázquez, Corros. Sci. 47 (2005) 795–809.
[8] S.R. Sánchez, Corros. Rev. 8 (1989) 283–332.
[9] F. Mansfeld, B. Little, Electrochim. Acta 37 (12) (1992) 2292–2297.
[10] J.R. Ibars, J.L. Polo, D.A. Moreno, C. Ranninger, J.M. Bastidas, Biotechnol. Bioeng. 87 (7) (2004) 855–861.
[11] P. Angell, A.H.L. Chamberlain, Int. Biodet. 27 (1991) 135–143.
[12] T.S. Rao, K.V. Nair, Corros. Sci. 40 (11) (1998) 1821–1836.
[13] M.M. Critchley, N.J. Cromar, N.C. McClure, H.J. Fallowfield, J. Appl. Microbiol. 94 (2003) 501–507.
[14] J. Morales, G.T. Fernandez, P. Esparza, S. Gonzalez, R.C. Salvarezza, M. Arévalo, Corros. Sci. 34 (9) (1993) 1531–1540.
[15] J.P. Busalmen, S.R. Sánchez, Appl. Environ. Microbiol. 64 (10) (1998) 3690–3697.
[16] J.P. Busalmen, M.B. Valcarce, S.R. Sánchez, Corros. Rev. 22 (4) (2004) 277–305.
[17] M.B. Valcarce, J.P. Busalmen, S.R. de Sánchez, Int. Biodeterior. Biodegrad. 50 (2002) 61–66.
[18] M. Stern, A.L. Geary, J. Electrochem. Soc. 104 (1957) 56.
[19] A. Palit, S. Pehkonen, Corros. Sci. 42 (2000) 1801–1822.
[20] J. Shim, J. Kim, Mater. Lett. 58 (2004) 2002–2006.
[21] L.J. Aljinovic, S. Gudic, M. Smith, J. Appl. Electrochem. 30 (2000) 973–979.
[22] R.E. Hummel, Phys. State Sol. (a) 76 (11) (1983) 12–43.
[23] S.R.d. Sánchez, L.E.A. Berlouis, D.J. Schiffrin, J. Electroanal. Chem. 307 (1991) 73.
[24] B.S. Kim, S.N. Piao, S.N. Hoier, S.M. Park, Corros. Sci. 37 (4) (1995) 557–570.
[25] C.H. Pyum, S.M. Park, J. Electrochem. Soc. 133 (10) (1986) 2024–2030.
[26] W.A. Badawy, S.S. El-Egamy, A.S. Azab, Corrosion 53 (11) (1997) 842–851.
[27] Y. Feng, W.K. Teo, K.S. Siow, A.K. Hsieh, Corros. Sci. 38 (1996) 387–395.
[28] H.W. Pickering, Corros. Sci. 23 (10) (1983) 1107.
[29] A.V. Vvedenskii, I.K. Marshakov, Electrochim. Acta 36 (5–6) (1991) 905.
[30] B. Assouli, A. Srhiri, H. Idrissi, NDT&E 36 (2) (2003) 117.
[31] G.T. Burstein, G. Gao, J. Electrochem. Soc. 141 (1994) 912.
[32] F.M. Al-Kharafi, B.G. Ateya, R.M.A. Allah, J. Appl. Electrochem. 33 (2003) 25–31.
[33] L. Burzynska, Corros. Sci. 43 (6) (2001) 1053.